IJMMM International Journal of Minerals, Metallurgy and Materials 矿物冶金与材料学报（英文版）

Optimization of ECAP–RAP process for preparing semisolid billet of 6061 aluminum alloy

Zu-jian Yang, Kai-kun Wang, and Yan Yang

Cite this article as:
Zu-jian Yang, Kai-kun Wang, and Yan Yang, Optimization of ECAP–RAP process for preparing semisolid billet of 6061 aluminum alloy, *Int. J. Miner. Metall. Mater.*, 27(2020), No. 6, pp. 792-800. https://doi.org/10.1007/s12613-019-1895-5

International Journal of Minerals, Metallurgy and Materials
Volume 27, Number 6, June 2020, Page 792
https://doi.org/10.1007/s12613-019-1895-5

Optimization of ECAP−RAP process for preparing semisolid billet of 6061 aluminum alloy

Zu-jian Yang[1)], *Kai-kun Wang*[1)], *and Yan Yang*[2)]

1) School of Materials Science and Engineering, University of Science and Technology Beijing, Beijing 100083, China
2) State Key Laboratory of Nickel and Cobalt Resources Comprehensive Utilization, Jinchang 737100, China
(Received: 10 July 2019; revised: 11 September 2019; accepted: 27 September 2019)

Abstract: 6061 aluminum alloy semisolid billet was prepared by the equal-channel angular processing (ECAP)−recrystallization and partial (RAP) process (a combination of equal-channel angular processing and recrystallization and partial remelting). The effects of different process parameters on the alloy microstructure were studied and the quantitative relationship between the process parameters and microstructure was established by response surface methodology (RSM) to optimize the process parameters. According to the orthogonal test, the holding temperature and holding time of the four ECAP−RAP process parameters were found to have the greatest impact on the microstructural characteristics, including average grain size and average shape factor. Through RSM, it was also found that when the average grain size or the average shape factor is optimized separately, another will be degraded. When the two indexes were simultaneously considered, the optimal process parameters were found to be a holding temperature of 623°C and holding time of 13 min, and the corresponding average grain size and average shape factor were 35.97 μm and 0.8535, respectively. Moreover, comparing the experimental and predicted values, the reliability of the established response surface model was verified.

Keywords: 6061 aluminum alloy; equal-channel angular pressing; semisolid microstructure; response surface methodology

1. Introduction

In recent years, semisolid metal forming technology, which combines the merits of casting and forging, has become a research hotspot in the field of metal processing [1]. It has several advantages such as a lower temperature requirement than casting, lower forming force than forging, high precision, and good quality of parts, achieving near-net-shape forming [2−3]. Aluminum alloy 6061 is a typical wrought alloy. The strengthening effect of the Mg_2Si phase makes the alloy possess superior comprehensive mechanical properties, which makes it widely used in important fields such as aviation, aerospace, and automobile [4−6]. However, the traditional forming process of 6061 aluminum alloy is "forging followed by machining", which has the disadvantages of low production efficiency, low material utilization rate, and high cost. If semisolid forming technology is used to realize a near-net-shape forming of the 6061 aluminum alloy, the aim of improving production efficiency, increasing material utilization, and reducing cost can be achieved [7−8].

The preparation of semisolid billet with fine and spheroidal grains is the first and key step of semisolid metal forming technology [9−10]. At present, the preparation methods of semisolid billets are mainly divided into liquid-state routes and solid-state routes [11]. Liquid-state routes mainly include the mechanical stirring method, electromagnetic stirring method, spray deposition method, and ultrasonic vibration method [12]. Compared with liquid-state routes, solid-state routes do not require a stirring process, and the prepared billet is pollution-free and highly dense. Therefore, solid-state routes for preparing semisolid billets have been widely studied. The solid-state routes mainly include the semisolid isothermal heat treatment, strain-induced melt activation (SIMA), and recrystallization and partial remelting (RAP), among which the latter two methods have been widely studied and applied [13−14]. The SIMA and RAP methods are very similar. Their ideas are to store distortion energy through plastic deformation and then to obtain semisolid billet by heating the deformed billet in semisolid temperature range. The minor difference between the two methods is that the plastic deformation temperature of the SIMA method is above the recrystallization temperature,

Corresponding author: Kai-kun Wang E-mail: kkwang@mater.ustb.edu.cn

while that of the RAP method is below the recrystallization temperature, and more often at room temperature [15]. Many researchers have prepared ideal semisolid billets by SIMA and RAP methods. Xue *et al.* [16] successfully prepared semisolid billets of Al–Si alloy with fine, uniform, and spherical grains by the SIMA method. Wang *et al.* [17] prepared ideal semisolid billets of AM60B magnesium alloy by the SIMA method and then used them for subsequent thixoforming. Finally, they obtained parts with good mechanical properties. Fu *et al.* [18] studied the effect of the heat treatment process of RAP on the semisolid microstructure of 7075 aluminum alloy and prepared ideal semisolid billets for subsequent thixoforming.

However, to date, the plastic deformation technologies used in the SIMA and RAP methods have been mostly traditional processes such as forging, extrusion, and rolling, which can only provide a limited amount of deformation. Consequently, the stored distortion energy of the deformed sample is relatively small, and the grain refinement effect is limited. By contrast, severe plastic deformation (SPD) techniques can provide a large enough deformation, and the effect of grain refining is remarkable, which can significantly improve the material strength and ductility [19−20]. Equal-channel angular processing (ECAP) as a typical SPD technique can provide a considerable amount of strain without changing the shape and size of the blank. Therefore, SIMA and RAP can be improved by introducing ECAP. In recent years, some researchers have introduced ECAP into the SIMA method or the RAP method to prepare semisolid billets and achieved good results [21−22].

To date, the studies on semisolid billets preparation mainly focus on the qualitative relationship between microstructure, properties, and process parameters [23−26], while the quantitative relationship between them has rarely been reported. In this paper, ECAP was introduced into the RAP method (ECAP−RAP process) to prepare 6061 aluminum alloy semisolid billet, the quantitative relationship between process parameters and microstructure was established by response surface methodology (RSM), and the parameters were optimized to obtain ideal semisolid billets of 6061 aluminum alloy.

2. Experimental

2.1. Materials

The feedstock material used in this study was a commercial 6061 aluminum alloy round bar, and its chemical composition is presented in Table 1. The semisolid temperature range and the liquid fraction−temperature relationship of the material were obtained by differential scanning calorimetry (DSC) thermal analysis. The semisolid temperature range was 591−653°C, and the liquid fraction−temperature relationship is shown in Fig. 1.

Table 1. Chemical composition of 6061 aluminum alloy wt%

Si	Fe	Ti	Cu	Mn	Mg	Cr	Zn	Al
0.5	0.7	0.15	0.25	0.15	1.0	0.15	0.25	Balance

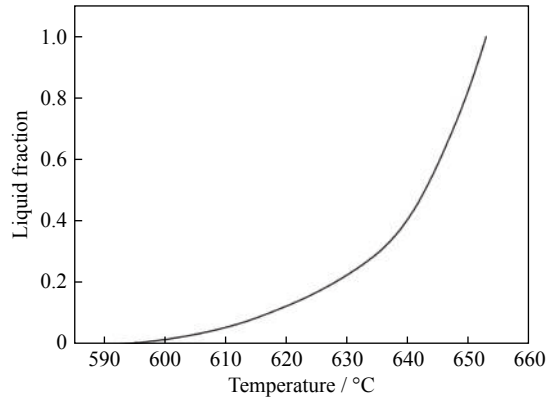

Fig. 1. Curve of liquid fraction vs. temperature of 6061 aluminum alloy.

2.2. ECAP−RAP process

Cylindrical billets with dimensions of 20 mm × 70 mm (diameter × length) were cut from the as-received materials for ECAP. Before the ECAP, homogenizing annealing for the billets is needed to improve the plasticity. In general, the homogenizing annealing temperature of aluminum alloy is between $0.9T_m$ and $0.95T_m$ (T_m is the solidus temperature of the material) [27]. After calculation, 540°C was chosen as the homogenizing annealing temperature. After homogenization at 540°C for 2 h, the billets were furnace-cooled to room temperature. Afterward, the homogenized billets were processed by ECAP with different numbers of ECAP passes and different ECAP routes at room temperature (as shown in Fig. 2). The pressing speed was 7 mm/s, and MoS_2 was used as the lubricant.

Samples with dimensions of 8 mm (length) × 8 mm (width) × 15 mm (thickness) were machined from the ECAP-deformed billets for semisolid heating to obtain semisolid billets. As for the RAP method, the liquid fraction of the samples should not exceed 40% when they are heated in the semisolid state. Therefore, a holding temperature of 600−630°C was selected in this study according to the curve of liquid fraction−temperature in Fig. 1, and the holding time was 5−35 min. The samples were heated by a PID-controlled resistance furnace, and their temperatures were monitored by a K-type thermometer system. The average heating rate of the sample in the furnace was 3.5°C/s, and when the samples reached the preset temperature, the holding time calculation began. After the holding time, the samples were quenched by water.

2.3. Microstructure characterization

The water-quenched samples were ground up to 5000 grit

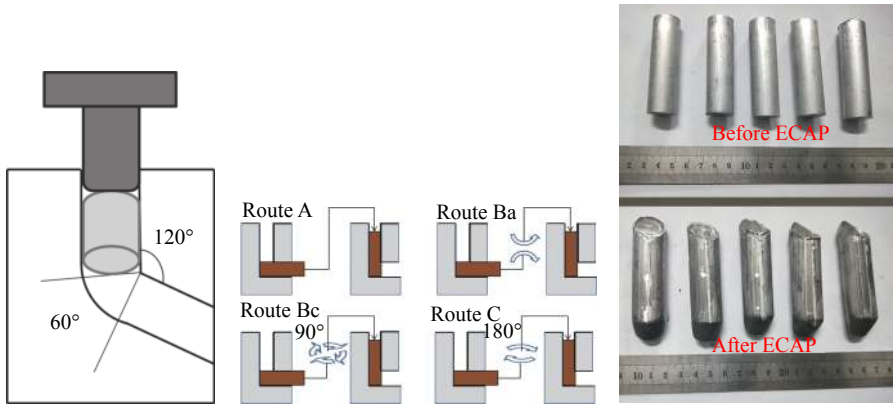

Fig. 2. ECAP process: (a) schematic illustration of ECAP; (b) ECAP routes; (c) samples before and after ECAP.

silicon carbide sandpaper and then electrolytically polished with an electrolyte (10 mL $HClO_4$, 90 mL C_2H_6O) at a voltage of 25 V for 15 s at room temperature. The polished surfaces of the samples were etched with Keller reagent for 30 s. The microstructures of the samples were observed and photographed by an optical microscope and analyzed by the Image-Pro Plus software. The average grain size (D) and the average shape factor (S_f) were calculated using Eqs. (1) and (2) [28–29], respectively:

$$D = \frac{\sum_{1}^{N} (4A/\pi)^{\frac{1}{2}}}{N} \tag{1}$$

$$S_f = \frac{\sum_{1}^{N} \left(4\pi A/P^2\right)}{N} \tag{2}$$

where D is the average grain size (μm), S_f is the average shape factor, A and P are respectively the area (μm^2) and perimeter of the grain (μm), and N is the number of grains.

3. Optimization of ECAP–RAP process using RSM

RSM is an optimum design method developed by the interaction of statistics, mathematics, and computer science. It can be used for the modeling and analysis of problems affected by many factors, and then, the optimal parameters to optimize the problems are sought [30–31]. Compared with the orthogonal test design, the RSM has several advantages; for example, it provides the relationship between response and influencing factors in a specified range, enables the study of the interaction of factors, and features high prediction accuracy [32]. If there are many influencing factors, we can first identify the significant factors through a range analysis of an orthogonal test design and then carry out the response surface design.

3.1. Orthogonal test design

The purpose of this orthogonal test design is to distinguish the significant parameters of the ECAP–RAP process on the semisolid microstructure of 6061 aluminum alloy and to pave the way for the response surface design. In this orthogonal test design, four levels of four factors were selected, and they include ECAP route, number of ECAP passes, holding temperature in semisolid temperature range, and holding time (as shown in Table 2). The average grain size and average shape factor calculated by Eqs. (1) and (2) were used as the inspection indexes. The scheme and results of the orthogonal test design are presented in Table 3, and the corresponding microstructures are shown in Fig. 3.

Table 2. Factors and levels for orthogonal test

Level	Factor			
	ECAP route	Number of ECAP passes	Holding temperature / °C	Holding time / min
1	A	1	600	5
2	Ba	2	610	15
3	Bc	3	620	25
4	C	4	630	35

The range analysis data of the two inspection indexes are presented in Table 4. In the table, the average value of the inspection index at each level are represented as K_1, K_2, K_3, K_4. Moreover, the range value (R) is also listed in Table 4 to evaluate the effect of each factor on the inspection index. The larger the R-value, the stronger the influence of this factor on the inspection index, and vice versa. As for the average grain size, the order of the R-value of the four factors is as follows: holding temperature > holding time > number of ECAP passes > ECAP route, which implies that the holding temperature and holding time have the greatest influence on the average grain size. Hence, these two factors are selected as variables to design the response surface model with the average grain size. Similarly, as for the average shape factor, the order of the R-value of four factors is as follows: holding tem-

Table 3. Scheme and results of the orthogonal test design

Test number	ECAP route	Number of ECAP passes	Holding temperature / °C	Holding time / min	Average grain size / μm	Average shape factor
1	A	1	600	5	33.99	0.5868
2	A	2	610	15	35.67	0.8265
3	A	3	620	25	43.80	0.7832
4	A	4	630	35	83.99	0.8318
5	Ba	1	610	25	38.17	0.7653
6	Ba	2	600	35	28.37	0.7246
7	Ba	3	630	5	34.64	0.8498
8	Ba	4	620	15	51.98	0.8529
9	Bc	1	620	35	50.81	0.7717
10	Bc	2	630	25	72.39	0.8145
11	Bc	3	600	15	25.05	0.7701
12	Bc	4	610	5	23.22	0.7723
13	C	1	630	15	56.28	0.8250
14	C	2	620	5	35.54	0.8156
15	C	3	610	35	53.35	0.6596
16	C	4	600	25	55.14	0.6845

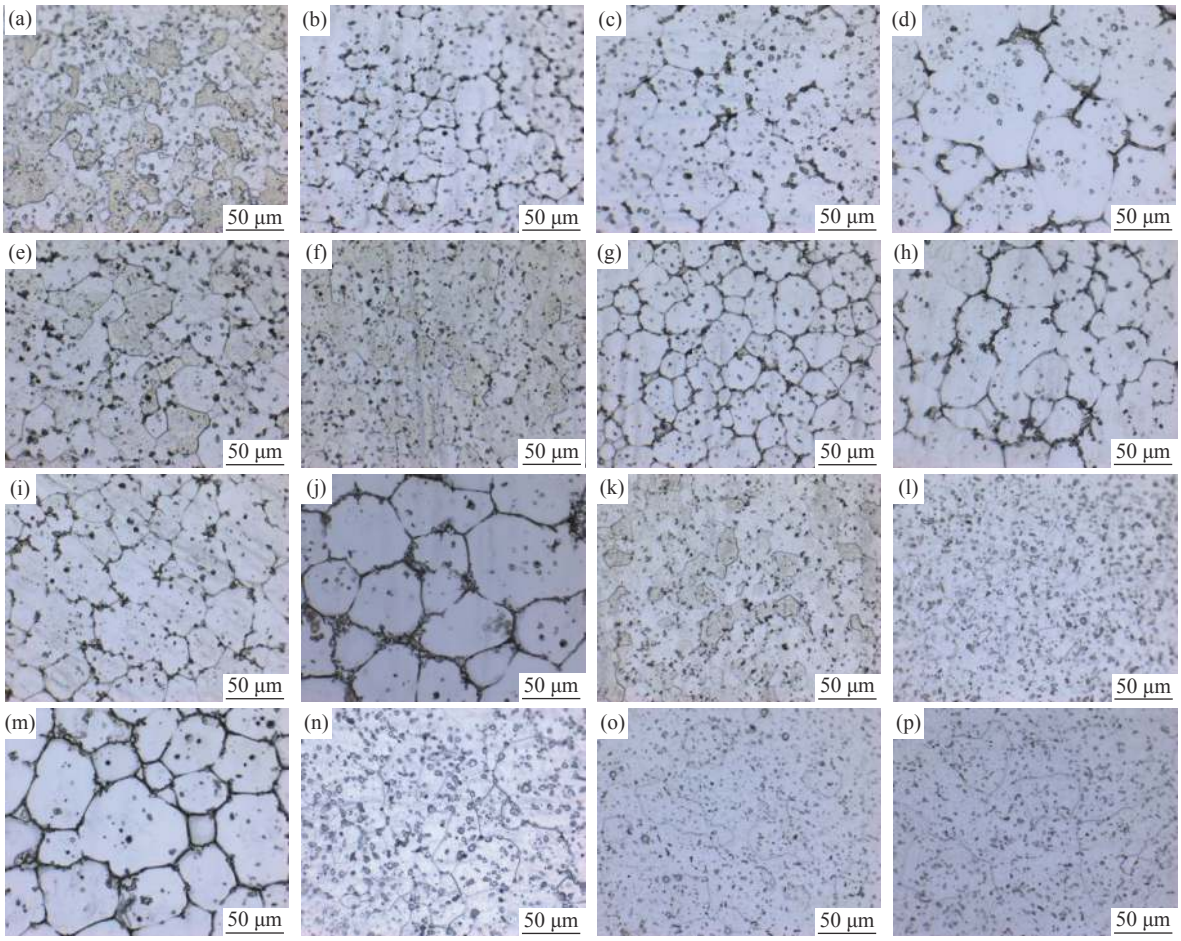

Fig. 3. Microstructures for orthogonal tests ((a–p) corresponding to tests Nos. 1–16 in Table 3, respectively).

perature > holding time > number of ECAP passes > ECAP route, which implies that the holding temperature and holding time have the greatest influence on the average shape factor. Hence, these two factors are selected as variables to design the response surface model with the average shape factor.

Table 4. Range analysis of average grain size and average shape factor

Factor	Average grain size / μm					Average shape factor				
	K_1	K_2	K_3	K_4	R	K_1	K_2	K_3	K_4	R
ECAP route	49.36	38.29	42.87	50.08	11.79	0.7571	0.7982	0.7822	0.7462	0.0520
Number of ECAP passes	44.81	42.99	39.21	53.58	14.37	0.7372	0.7953	0.7657	0.7854	0.0581
Holding temperature	35.64	37.60	45.53	61.83	26.19	0.6915	0.7559	0.8059	0.8303	0.1388
Holding time	31.85	42.25	52.38	54.13	22.28	0.7561	0.8186	0.7619	0.7469	0.0717

3.2. Response surface design

3.2.1. Establishment of response surface model

According to the results of the orthogonal test analysis, the holding temperature and holding time are both significant factors affecting the average grain size and the average shape factor. Therefore, these two factors are taken as design variables, the average grain size and the average shape factor are taken as responses, and Design-Expert 11 software is used as a tool to design the response surface model. As shown in Fig. 3, the recrystallization process was not complete enough when the holding temperature was 600°C. Considering this, the holding temperature selected in this response surface design was 610−630°C and the time was 10−30 min. The scheme and results of response surface design are shown in Table 5, and the corresponding microstructures are shown in Fig. 4.

Table 5. Scheme and results of the response surface design

Test number	Holding temperature / °C	Holding time / min	Average grain size / μm	Average shape factor
1	610	10	24.50	0.7158
2	634	20	76.62	0.8749
3	620	6	30.93	0.8188
4	620	20	33.79	0.8447
5	620	20	33.36	0.8497
6	620	20	34.82	0.8332
7	620	20	35.54	0.8317
8	610	30	29.46	0.7877
9	606	20	26.89	0.7417
10	620	34	47.14	0.8109
11	630	10	53.49	0.8765
12	630	30	102.36	0.8566
13	620	20	34.12	0.8268

3.2.2. Analysis of response surface model

According to the results presented in Table 5, the regression equations between the responses and the two variables were established by Design-Expert 11 software as follows:

$$\frac{1}{D} = 0.0291 - 0.0085T - 0.0039t - 0.0005Tt - 0.002T^2 - 0.0012t^2 - 0.003Tt^2 \quad (3)$$

$$S_f = 0.8372 + 0.0471T - 0.0028t - 0.0229Tt - 0.0151T^2 - 0.0118t^2 + 0.0158T^2t + 0.0103Tt^2 \quad (4)$$

where D is the average grain size (μm), S_f is the average shape factor, T is the holding temperature (°C), and t is the holding time (min).

To access the reliability and accuracy of the response surface models, the variance analysis of each model was carried out and the results are presented in Tables 6 and 7. It can be seen from Table 6 that the response surface model of the average grain size is significant ($P < 0.0001$) and the lack of fit of the model is not significant (0.9634 > 0.05). The values of the determination coefficient (R^2), adjusted determination coefficient (adjusted R^2) and predicted determination coefficient (predicted R^2) are 0.9978, 0.9956, and 0.9956, respectively, which are close to 1. Moreover, the signal-to-noise ratio (adequate precision) is 70.5399, far greater than 4. The above analysis indicates that regression Eq. (3) has a high degree of fit with the test data and that the response surface model of the average grain size has a high reliability and can be used for the average grain size prediction. Similarly, Table 7 shows that the response surface model of the average shape factor is significant ($P = 0.0002 < 0.05$) and that the lack of fit of the model is not significant (0.7384 > 0.05). The values of the determination coefficient (R^2), adjusted determination coefficient (adjusted R^2), and predicted determination coefficient (predicted R^2) are 0.9862, 0.9670, and 0.9518, respectively, which are close to 1, and the signal-to-noise ratio (adequate precision) is 23.5395, far greater than 4. The above analysis indicates that regression Eq. (4) has a high degree of fit with the test data and that the response surface model of the average shape factor has a high reliability and can be used for the prediction of the average shape factor.

The 3D surface of the influence of the holding temperature and holding time on the average grain size is shown in Fig. 5. It can be found that the effect of the interaction between the holding temperature and holding time on the average grain size is not remarkable, which can also be reflected by the P-value of the Tt-term in Table 6 (0.1376 > 0.05). Moreover, it can be also found that the average grain size increases with the increase of the holding temperature and holding time. According to the prediction of the response surface model, the minimum value of the average grain size is 24.50 μm and the corresponding process parameters are a holding temperature of 610°C and a holding time of 10 min. At this time, the predicted value of the average shape factor is 0.7179.

The 3D surface of the influence of the holding temperature and holding time on the average shape factor is shown in

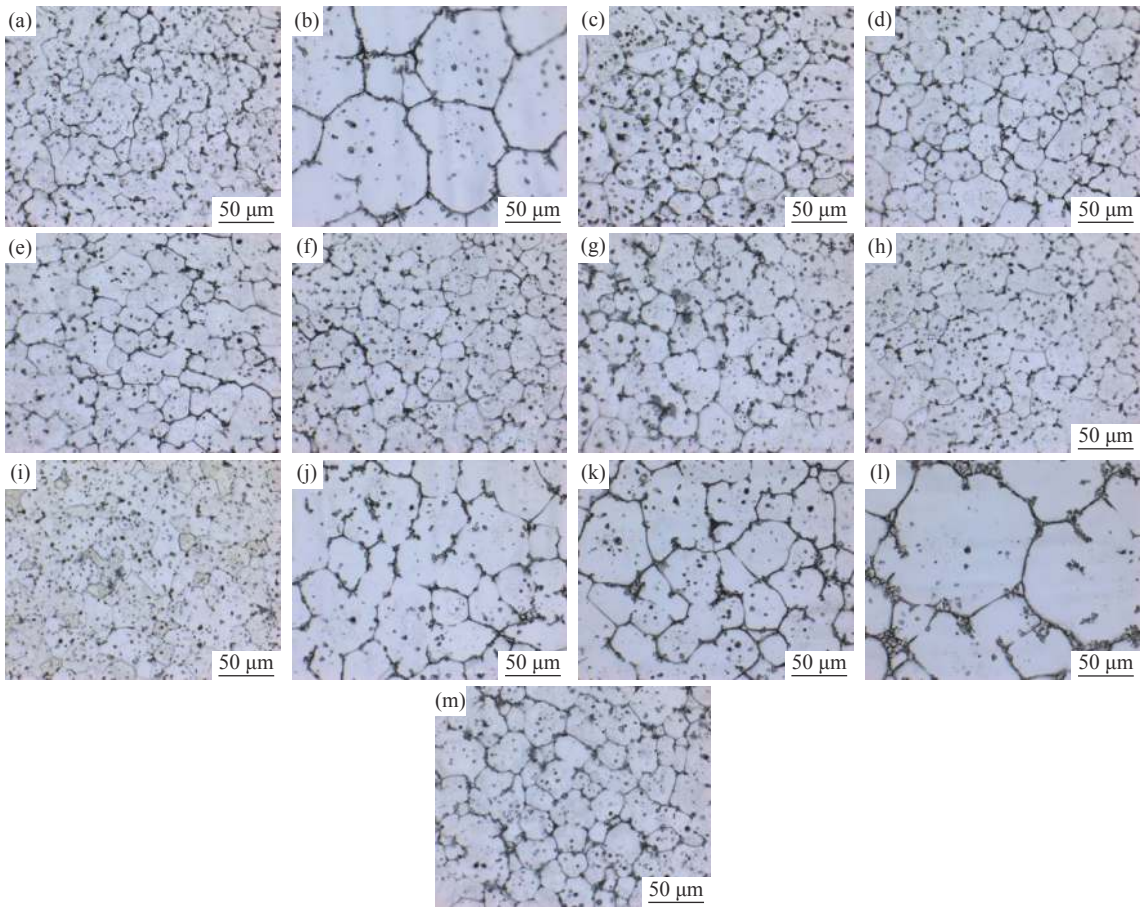

Fig. 4. Microstructures for response surface design ((a–m) corresponding to tests Nos. 1–13 in Table 5, respectively).

Table 6. Analysis of variance of the average grain size

Source	Sum of squares	Degree of freedom	Mean square	*F*-value	*P*-value	Significance
Model	9.98×10^{-4}	6	1.65×10^{-4}	458.28	<0.0001	Yes
Holding temperature (T)	2.91×10^{-4}	1	2.91×10^{-4}	810.69	<0.0001	—
Holding time (t)	1.24×10^{-4}	1	1.24×10^{-4}	345.63	<0.0001	—
Tt	1.05×10^{-6}	1	1.05×10^{-6}	2.93	0.1376	—
T^2	2.92×10^{-5}	1	2.92×10^{-5}	81.24	0.0001	—
t^2	1.04×10^{-5}	1	1.04×10^{-5}	28.93	0.0017	—
Tt^2	1.85×10^{-5}	1	1.85×10^{-5}	51.45	0.0004	—
Residual	2.16×10^{-6}	6	3.59×10^{-7}	—	—	—
Lack of fit	3.98×10^{-8}	2	1.99×10^{-8}	0.04	0.9634	No
Pure error	2.12×10^{-6}	4	5.29×10^{-7}	—	—	—
Corrected total	9.90×10^{-4}	12	—	—	—	—
$R^2 = 0.9978$	Adjusted $R^2 = 0.9956$		Predicted $R^2 = 0.9956$		Adequate precision = 70.5399	

Fig. 6. It can be found that the effect of the interaction between the holding temperature and holding time on the average shape factor is remarkable, which can also be reflected by the *P*-value of the *Tt*-term in Table 7 (0.0033 < 0.05). Moreover, it can be also found that the large average shape factor mainly concentrates in the higher-temperature region. According to the prediction of the response surface model, the maximum value of the average shape factor is 0.8767, and the corresponding process parameters are a holding temperature of 630°C and a holding time of 11 min. At this time, the predicted value of the average grain size is 51.63 μm.

3.3. Simultaneous optimization of two responses and its verification

According to the analysis in the previous section, when the average grain size or the average shape factor was optimized separately, another will be degraded. To address this problem, the two indexes were optimized simultaneously

Table 7. Analysis of variance of the average shape factor

Source	Sum of squares	Degree of freedom	Mean square	*F*-value	*P*-value	Significance
Model	2.71×10^{-2}	7	3.88×10^{-3}	51.17	0.0002	Yes
Holding temperature (T)	8.87×10^{-3}	1	8.87×10^{-3}	117.14	0.0001	—
Holding time (t)	3.00×10^{-5}	1	3.00×10^{-5}	0.41	0.5492	—
Tt	2.11×10^{-3}	1	2.11×10^{-3}	27.82	0.0033	—
T^2	1.58×10^{-3}	1	1.58×10^{-3}	20.85	0.0060	—
t^2	9.70×10^{-4}	1	9.70×10^{-4}	12.77	0.0160	—
T^2t	5.00×10^{-4}	1	5.00×10^{-4}	6.59	0.0503	—
Tt^2	2.10×10^{-4}	1	2.10×10^{-4}	2.81	0.1548	—
Residual	3.80×10^{-4}	5	8.00×10^{-5}	—	—	—
Lack of fit	1.00×10^{-5}	1	1.00×10^{-5}	0.13	0.7384	No
Pure error	3.70×10^{-4}	4	9.00×10^{-5}	—	—	—
Corrected total	2.75×10^{-2}	12	—	—	—	—
$R^2 = 0.9862$	Adjusted $R^2 = 0.9670$		Predicted $R^2 = 0.9518$		Adequate precision = 23.5395	

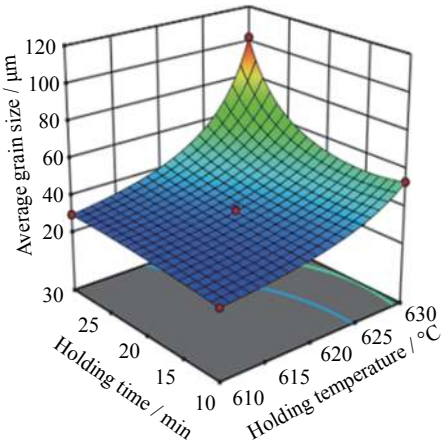

Fig. 5. Response surface of process parameters on average grain size.

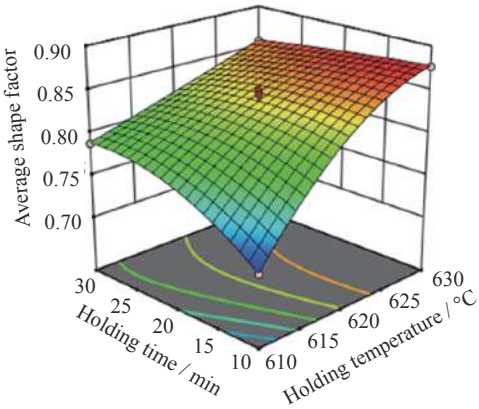

Fig. 6. Response surface of process parameters on average shape factor.

based on the two response surface models, and the optimum process parameters are a holding temperature of 623°C and a holding time of 13 min. The corresponding prediction results are an average grain size of 35.97 μm and an average shape factor of 0.8535.

The experiment was carried out with the holding temperature of 623°C and the holding time of 13 min, and the microstructure obtained is shown in Fig. 7. The obtained average grain size and average shape factor are 36.79 μm and 0.8600, respectively, and the corresponding errors between the experimental and predicted values are 2.27% and 0.76%, respectively. The errors are small enough, which verifies the reliability of the response surface models.

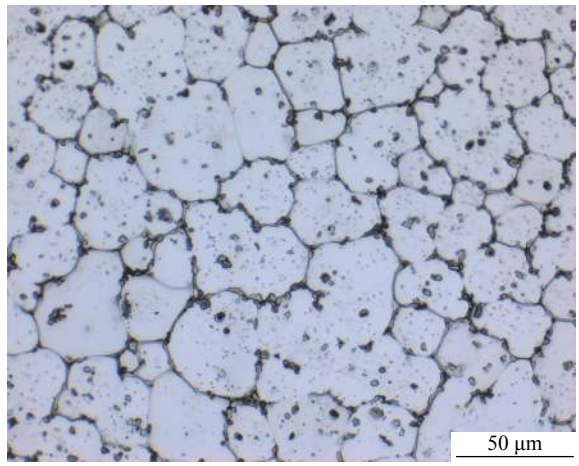

Fig. 7. Microstructure of optimum conditions resulting from response surface methodology (623°C, 13 min).

4. Conclusions

(1) According to DSC thermal analysis, the solidus and liquidus of as-received 6061 aluminum alloy were found to be 591°C and 653°C, respectively; that is, the semisolid temperature range of the materials is 591−653°C.

(2) According to the results of the orthogonal test analysis, the holding temperature and holding time of the four ECAP−RAP process parameters are both significant factors affecting the average grain size and average shape factor.

(3) Through response surface design, when the average grain size or the average shape factor is optimized separately, another will be degraded. When the two indexes were considered simultaneously, the optimum process parameters were found to be a holding temperature of 623°C and a holding time of 13 min, and the corresponding average grain size and average shape factor are 35.97 μm and 0.8535, respectively.

(4) The errors between the experimental values and the predicted values of the response surface models are small enough, which verifies the reliability of the response surface model.

Acknowledgements

This study was financially supported by the National Key Research and Development Program of China (Nos. 2017YFB0701803 and 2016YFB0701403) and the State Key Laboratory of Nickel and Cobalt Resources Comprehensive Utilization, China.

References

[1] Y.N. Chen, G. Liu, X.M. Zhang, and Y.Q. Zhao, Influence of semisolid forging ratio on the microstructure and mechanical properties of Ti14 alloy, *Int. J. Miner. Metall. Mater.*, 20(2013), No. 3, p. 266.

[2] W. Liu, D.D. Yang, G.F. Quan, Y.B. Zhang, and D.D. Yao, Microstructure evolution of semisolid Mg−2Zn−0.5Y alloy during isothermal heat treatment, *Rare Met. Mater. Eng.*, 45(2016), No. 8, p. 1967.

[3] M.J. Nayyeri and K. Dehghani, Microstructure evolution in as-cast and SIMA-processed AE42 magnesium alloy, *J. Mater. Eng. Perform.*, 23(2014), No. 9, p. 3077.

[4] D.T. Wang, H.T. Zhang, L. Li, H.L. Wu, K. Qin, and J.Z. Cui, The evolution of microstructure and mechanical properties during high-speed direct-chill casting in different Al−Mg_2Si *in situ* composites, *Int. J. Miner. Metall. Mater.*, 25(2018), No. 9, p. 1080.

[5] F. Ozturk, A. Sisman, S. Toros, S. Kilic, and R.C. Picu, Influence of aging treatment on mechanical properties of 6061 aluminum alloy, *Mater. Des.*, 31(2010), No. 2, p. 972.

[6] M. Mansourinejad and B. Mirzakhani, Influence of sequence of cold working and aging treatment on mechanical behaviour of 6061 aluminum alloy, *Trans. Nonferrous Met. Soc. China*, 22(2012), No. 9, p. 2072.

[7] Q. Chen, Z.D. Zhao, G. Chen, and B. Wang, Effect of accumulative plastic deformation on generation of spheroidal structure, thixoformability and mechanical properties of large-size AM60 magnesium alloy, *J. Alloys Compd.*, 632(2015), p. 190.

[8] C.Q. Zhao and R.B. Song, Evolution of microstructure and mechanical properties for 9Cr18 stainless steel during thixoforming, *Mater. Des.*, 59(2014), p. 502.

[9] S.Z. Shang, G.M. Lu, X.L. Tang, Z.X. Zhao, and C.M. Wu, Deformation mechanism and forming properties of 6061Al alloys during compression in semi-solid state, *Trans. Nonferrous Met. Soc. China*, 20(2010), No. 9, p. 1725.

[10] Y. Xu, J.B. Jia, C. Chen, W.C. Liu, S.Y. Luo, Y. Yang, and L.X. Hu, Thixoforming of semi-solid AZ91D alloy with high solid fraction prepared by the RUE-based SIMA process, *Int. J. Adv. Manuf. Technol.*, 93(2017), No. 9-12, p. 4317.

[11] F. Wang, W.Q. Zhang, W.L. Xiao, H. Yamagata, and C.L. Ma, Microstructural evolution during reheating of A356 machining chips at semisolid state, *Int. J. Miner. Metall. Mater.*, 24(2017), No. 8, p. 891.

[12] H.V. Atkinson, Modelling the semisolid processing of metallic alloys, *Prog. Mater. Sci.*, 50(2005), No. 3, p. 341.

[13] C.P. Wang, Z.J. Tang, H.S. Mei, L. Wang, R.Q. Li, and D.F. Li, Formation of spheroidal microstructure in semi-solid state and thixoforming of 7075 high strength aluminum alloy, *Rare Met.*, 34(2015), No. 10, p. 710.

[14] R. Meshkabadi, G. Faraji, A. Javdani, A. Fata, and V. Pouyafar, Microstructure and homogeneity of semi-solid 7075 aluminum tubes processed by parallel tubular channel angular pressing, *Met. Mater. Int.*, 23(2017), No. 5, p. 1019.

[15] J.F. Jiang, Y. Wang, and H.V. Atkinson, Microstructural coarsening of 7005 aluminum alloy semisolid billets with high solid fraction, *Mater. Charact.*, 90(2014), p. 52.

[16] K.M. Xue, G.B. Mi, and Q.R. Wang, Compound fabrication technology of semi-solid billet of Al−Si alloy based on SIMA method, *Trans. Nonferrous Met. Soc. China*, 16(2006), No. 3, p. 1224.

[17] L.P. Wang, W.Y. Jiang, T. Chen, Y.C. Feng, H.Y. Zhou, S.C. Zhao, Z.Q. Liang, and Y. Zhu, Spheroidal microstructure formation and thixoforming of AM60B magnesium alloy prepared by SIMA process, *Trans. Nonferrous Met. Soc. China*, 22(2012), p. 435.

[18] J.L. Fu, K.K. Wang, X.W. Li, and H.K. Zhang, Microstructure evolution and thixoforming behavior of 7075 aluminum alloy in the semi-solid state prepared by RAP method, *Int. J. Miner. Metall. Mater.*, 23(2016), No. 12, p. 1404.

[19] A.A. Khamei, K. Dehghani, and R. Mahmudi, Modeling the hot ductility of AA6061 aluminum alloy after severe plastic deformation, *JOM*, 67(2015), No. 5, p. 966.

[20] T. Yuan, J.H. Jiang, L.S. Wang, and A.B. Ma, Overview on the microstructure and mechanical properties of ultrafine-grained Al−Li alloys produced by severe plastic deformation, *Rare Met. Mater. Eng.*, 48(2019), No. 1, p. 55.

[21] M. Aghaie-Khafri and D. Azimi-Yancheshme, The Study of an Al−Fe−Si alloy after equal-channel angular pressing (ECAP) and subsequent semisolid heating, *JOM*, 64(2012), No. 5, p. 585.

[22] K.N. Campo and E.J. Zoqui, Thixoforming of an ECAPed aluminum A356 alloy: Microstructure evolution, rheological behavior, and mechanical properties, *Metall. Mater. Trans. A*, 47(2016), No. 4, p. 1792.

[23] J.L. Fu, H.J. Jiang, and K.K. Wang, Influence of processing parameters on microstructural evolution and tensile properties for 7075 Al alloy prepared by an ECAP-based SIMA process, *Acta Metall. Sin.*, 31(2018), No. 4, p. 337.

[24] R. Meshkabadi, G. Faraji, A. Javdani, and V. Pouyafar, Combined effects of ECAP and subsequent heating parameters on semi-solid microstructure of 7075 aluminum alloy, *Trans. Nonferrous Met. Soc. China*, 26(2016), No. 12, p. 3091.

[25] A. Bolouri, M. Shahmiri, and C.G. Kang, Study on the effects of the compression ratio and mushy zone heating on the thixotropic microstructure of AA 7075 aluminum alloy via SIMA process, *J. Alloys Compd.*, 509(2011), No. 2, p. 402.

[26] L. Zhang, Y.B. Liu, Z.Y. Cao, Y.F. Zhang, and Q.Q. Zhang, Effects of isothermal process parameters on the microstructure of

semisolid AZ91D alloy produced by SIMA, *J. Mater. Process. Technol.*, 209(2009), No. 2, p. 792.

[27] H.L. Zhang, X. Li, S.Q. Xiang, C.R. Zhou, and Y.H. Cai, Alloying principle and its application in production of 6××× series wrought aluminum alloy (in Chinese), *Light Alloy Fabr. Technol.*, 40(2012), No. 3, p. 12.

[28] J.F. Jiang, Y. Wang, J.J. Qu, Z.M. Du, Y. Sun, and S.J. Luo, Microstructure evolution of AM60 magnesium alloy semisolid slurry prepared by new SIMA, *J. Alloys Compd.*, 497(2010), No. 1-2, p. 62.

[29] Y.F. Wang, S.D. Zhao, X.Z. Zhao, and Y.Q. Zhao, Microstructural coarsening of 6061 aluminum alloy semi-solid billets prepared via recrystallization and partial melting, *J. Mech. Sci. Technol.*, 31(2017), No. 8, p. 3917.

[30] J. Grum and J.M. Slabe, The use of factorial design and response surface methodology for fast determination of optimal heat treatment conditions of different Ni−Co−Mo surfaced layers, *J. Mater. Process. Technol.*, 155-156(2004), p. 2026.

[31] M.A. Bezerra, R.E. Santelli, E.P. Oliveira, L.S. Villar, and L.A. Escaleira, Response surface methodology (RSM) as a tool for optimization in analytical chemistry, *Talanta*, 76(2008), No. 5, p. 965.

[32] D. Baş and İ.H. Boyacı, Modeling and optimization I: Usability of response surface methodology, *J. Food Eng.*, 78(2007), No. 3, p. 836.